# Preliminary assessment of the environmental impact of space debris demise during atmospheric reentry

**José P. Ferreira and Joseph Wang**
*Department of Astronautical Engineering, University of Southern California*

**Ken-ichi Nomura**
*Department of Chemical Engineering and Materials Science, University of Southern California*

## ABSTRACT

The number of orbiting satellites has increased significantly in an unrestricted and unregulated manner over the last decades, threatening the sustainable access to space in the future. Ongoing plans to build mega-constellations of microsatellites will inevitably increase the number of orbiting bodies, adding up to the ever-growing number of pieces of debris. Reentry rates are expected to continue growing as the number of orbiting bodies increases with more satellites and launch vehicle remainings in orbit. While it is widely understood that most objects will completely burn during reentry, the effect of space debris demise on Earth's atmosphere has only been lightly studied and the long-term impact remains unknown. We resort to reactive molecular dynamics simulations to resolve the oxidation process of the key structural material of aluminum for mesospheric reentry, herewith presenting the first large-scale supercomputer runs on the generation of aluminum oxide nanoparticles. As of 2022, the total mass of re-entering objects from Low-Earth Orbit (LEO) summed up to 309 metric tons, resulting in an 18 % increase when compared with the previous year. On its own, it already consists in an 87 % increase of the yearly mass rate of aluminum injected at the top of the atmosphere when compared with natural sources. Results show that aluminum oxides resulting from space debris demise in the mesosphere cluster into nanoparticles and take decades decaying to lower altitudes.

## 1. BACKGROUND

Earth's orbit presents around 60 % of mission-related debris, rocket stage remainings, and defunct spacecraft; and 40 % of debris fragments that were primarily originated by any of the previous forms [1]. This is thoroughly explained by a model firstly defined as the *Kessler Syndrome* in the late 1970s [2], bringing to light the need to declutter such environment. Empirical data from 2022 shows that there are more than 34,000 pieces of debris larger than 10 centimeters across – population which is expected to double every 75 years – while reentries from Low-Earth Orbit (LEO) summed up to 146.3 and 162.6 metric tons for satellites and launch vehicles, respectively [3]. Rough estimations of future reentry rates for LEO and other orbits point to 800 to 3200 metric tons per year for satellites, and up to 1000 metric tons per year for launch vehicles [4]. The overall imbalance of launched and reentered objects on a yearly basis can be appreciated in Table 1, where a clear trend of increasing satellite and launch vehicle mass launched is unmatched by the mass fraction reentered.

The only observational study representative of a spacecraft reentering from LEO was conducted more than a decade ago in a joint effort between ESA and NASA. This campaign gathered valuable data from the reentry of the ATV-1 cargo resupply vehicle, producing one of the most valuable pieces of empirical evidence to date, showing presence of aluminum and other metals during reentry at an altitude of 74 km [5]. In 2021, ESA published two computational studies on the assessment of pollutants from spacecraft demise during reentry. The ATISPADE study [6] showed a coarse estimation of atmospheric emissions of a 20-metric-ton spacecraft, estimating reentry byproducts such as nitrogen oxides and chlorine; while the ARA study [7] considered the demise of structural panels during reentry to estimate the byproduct generation of nitrogen, aluminum, and titanium oxides in the mesosphere. In spite of the polluting potential, it was concluded that the atmospheric impact of spacecraft reentries is relatively low when compared with that of aviation or road transportation, although uncertainties on the byproduct generation and transportation modelling persist along with lack of observational data to validate the models.

In tandem, there is an increasing need for answers from regulatory bodies. The FCC emphasized, in April 2021, the «Potential Effect on Earth's Atmosphere from Satellite Launch and Reentry» while reviewing Starlink's batch 1 modification application [6]. It was argued that such satellites, built from aluminum, could generate aluminum oxides during reentry, which is a climate change potentiator. However, lack of evidence prevented subsequent regulatory actions. In December 2022, the FCC conceded partial approval of Starlink generation 2 satellites based on the environmental impact estimations presented in the aforementioned studies by ESA, although future approvals are conditioned to the operator's «commitment [...] to explore methods to collect observational data on the formation of alumina from satellite reentry».

While the computational studies abovementioned provide valuable inputs to assess the macroscopic generation of chemicals during re-entry, such methods are based on the understanding of the reentry phenomena until breakup. An in-depth understanding of the process at an atomic scale shall provide better clarity as to what happens after the spacecraft demises with the impact of an increasingly denser atmosphere. The approach herewith presented follows up on the proposed methodology developed by the authors of this manuscript with preliminary results briefly summarized in [8] [9].

Table 1. Yearly mass count for reentered objects originated in LEO, including Satellite- and Launch Vehicle-related bodies, where the summation of both categories is depicted under *Total*. All mass values are presented in metric tons. Data retrieved from [3][*].

| Year | Launched mass | | | Reentered mass | | |
|---|---|---|---|---|---|---|
| | Satellites | Launch Vehicles | Total | Satellites | Launch Vehicles | Total |
| 2016 | 122.6 | 66.5 | 189.1 | 18.8 | 103 | 121.8 |
| 2017 | 189.6 | 71.4 | 261.0 | 13.0 | 59.0 | 72.0 |
| 2018 | 195.7 | 76.6 | 272.3 | 33.3 | 55.8 | 89.1 |
| 2019 | 215.3 | 62.3 | 277.6 | 57.5 | 93.7 | 151.2 |
| 2020 | 410.1 | 89.5 | 499.6 | 74.7 | 100.6 | 175.3 |
| 2021 | 648.9 | 144.1 | 793.0 | 110.4 | 151.7 | 262.1 |
| 2022 | 826.6 | 219.4 | 1046.0 | 146.3 | 162.6 | 308.9 |

## 2. METHODOLOGY

### 2.1 Approach

A Molecular Dynamics (MD) simulation study on the atmospheric chemical mechanisms is presented to resolve the byproducts generated by space debris reentry. This tool emulates the interaction between atoms by considering the interatomic potentials and external forces at each time step, which are directly simulated at very reduced length scales. The Reactive Force Field (ReaxFF) [10] is used to describe the chemical bond breakage and formation, having been extensively used in the material science domain to study the oxidation process of metals and hypervelocity impacts. The simulations herewith presented rely on empirically generated force fields that describe the behavior of an Aluminum-Oxygen system [11], resorting to the Reactive Molecular Dynamics (RXMD) framework [12] that optimizes ReaxFF for time-effective parallel simulations by following the time evolution of atomic trajectories.

[*]Satellite-related data covers the categories defined in [3] as *Payload* (PL), *Payload Fragmentation Debris* (PF), *Payload Debris* (PD), and *Payload Mission Related Object* (PM); while Launch Vehicle-related data concerns *Rocket Body* (RB), *Rocket Fragmentation Debris* (RF), *Rocket Debris* (RD), and *Rocket Mission Related Object* (RM)

The goal is to resolve the bond breakage between aluminum atoms (Al-Al bonds) due to the impact of oxygen molecules (O-O bonds) and the formation of aluminum oxides (Al-O bonds) under mesospheric reentry conditions from LEO. To that end, the simulation accounts for the impact of oxygen molecules during the ablation stage of reentry and runs until the number of Al-O bonds stabilizes. The output retrieved consists of the atomic position and velocity which can be used to define several clusters made out of aluminum oxides (AlO) and aluminum (Al). The mass of each cluster is defined by accounting for the atomic mass of each species, then used to compute the aerodynamic diameter ($d_a$) as the cluster characteristic length [13].

The aerodynamic diameter is considered to be a standard normal variable. A log-normal distribution – the standard to describe natural growth process in the atmosphere – is defined as the probability distribution of the variable $X$ presented in Equation 1, where $\mu_X$ is the mean and $\sigma_X$ the standard deviation (often referred to as *shape parameter*) of the natural logarithm of $X$.

$$X = e^{\mu_X + \sigma_X d_a} \tag{1}$$

The probability distribution of the natural logarithm of $X$ – a log-normal Probability Density Function (PDF) – satisfies Equation 2 for $x > 0$, $\sigma_X > 0$, $\mu_X \in [-\infty, +\infty]$. The following notation is used for the mean $E(Z)$, mode $M(Z)$, and standard deviation $SD(Z)$ of a distribution of any variable $Z$.

$$f_X(x) = \frac{1}{x\sigma_X\sqrt{2\pi}} e^{-\frac{\ln^2(x-\mu_X)}{2\sigma^2}} \tag{2}$$

Then, the settling time of each cluster can be estimated resorting to a one-dimensional atmospheric model based on the U.S. Standard Atmosphere [14] that accounts for viscous forces ($F_v$) as per Stokes' Law corrected for high Knudsen numbers ($K_n$) through the Cunnigham Correction factor ($C_c$), depicted in Equation 3:

$$\overrightarrow{F_v} = -\frac{3\pi\mu d_a}{C_c}\vec{v} \tag{3}$$

where $d_a$ is the cluster's aerodynamic diameter, $v$ is the velocity, and $\mu$ is the atmospheric kinematic viscosity as a function of altitude. The Cunnigham Correction factor accounts for non-continuum effects when calculating viscous forces acting on small particles up to mesospheric pressure levels, defined in Equation 4 [15].

$$C_c = 1 + K_n\left(1.102 + 0.4e^{-\frac{1.144}{K_n}}\right) \tag{4}$$

Assuming steady state conditions and no further mass loss after the thermal ablation stage emulated in the MD simulations, iteratively solving the force balance between the cluster weight and viscous forces provides the solution to a first-order linear ordinary differential equation. The cluster velocity is then used to compute the settling time with respect to a reference altitude.

## 2.2 Setup

The benchmark of this case study is a generic box of 250 kg and dimensions of 3.2 × 1.6 × 0.2 m$^3$. As the object has its origin in LEO and the high-temperature stage of reentry is dominated by thermal ablation at temperatures in excess of 2000 K, a worst-case scenario is designed for 90 seconds at constant attitude coinciding with the largest wetted area. The molecular oxygen number density is set to $3 \times 10^{19}$ m$^{-3}$, while aluminum is structured in a Face-Centered Cubic form with lattice constant of $4.03893 \times 10^{-10}$ m and the (111) surface exposed to the incoming flow. The molar ratio between the reactants oxygen and aluminum ($R_{O/Al}$) in this reentry scenario is of 0.1294, with the overall setup presented in Fig. 1.

The MD simulation is carried out in a downsized domain with periodic boundary conditions comprising a varying set of aluminum ($N_{Al}$) and oxygen ($N_O$) atoms – and consequentially surface area ($\boldsymbol{S}$) – as depicted in Table 2. The number of atoms increases one order of magnitude from cases A to D while roughly keeping the same molar ratio so as to assess the variability of the PDF outputted from the MD simulation, then used to compute the settling time of the expected cluster size in the atmosphere.

Table 2. Atomic count and surface area for simulation cases A through D

| Case | $\boldsymbol{N_{Al}}$ | $\boldsymbol{N_O}$ | $\boldsymbol{R_{O/Al}}$ | $\boldsymbol{S} \times 10^{-20}$ [m$^2$] |
|---|---|---|---|---|
| A | 1360 | 176 | 0.1294 | 50 × 26 |
| B | 2772 | 358 | 0.1291 | 61 × 31 |
| C | 6720 | 870 | 0.1295 | 81 × 41 |
| D | 13,300 | 1722 | 0.1295 | 101 × 51 |

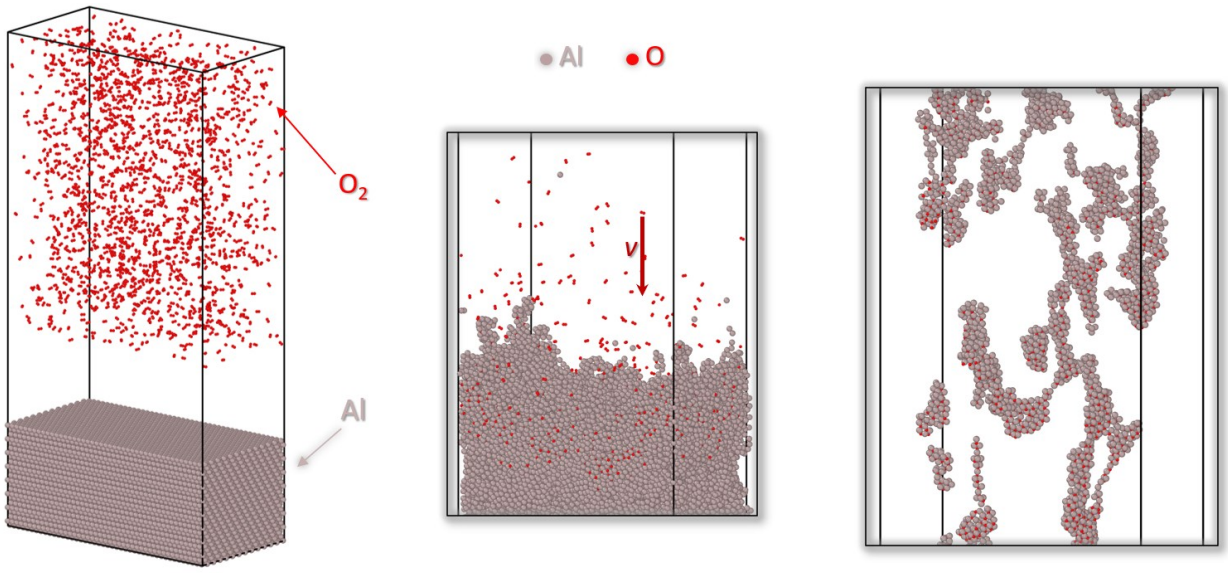


(i) (ii) (iii)

Fig. 1. Snapshots from the MD simulation, generated through the Open Visualization Tool (OVITO) [16]: (i) initial configuration of molecular oxygen and aluminum, (ii) impingement of molecular oxygen into the aluminum structure, (iii) generation of clusters of aluminum (gray atoms) and aluminum oxides (red and gray atoms).

## 3. RESULTS

Considering the yearly reentry figures from LEO provided in Table 1, it is possible to estimate the aluminum mass fraction that reentered the atmosphere since 2016. For satellites, 30 % of the total mass is considered to be structural and made of aluminum – median mass fraction value between [17] and [18] – with a survivability to reentry of 5 % [18]. As to launch vehicles, 77 % of the mass fraction is considered to be aluminum [18], with reentry survivability of 35 % - the recovered Delta II second stage is taken as a benchmark [19]. Notwithstanding, there are natural sources such as meteoroids injecting this same metallic component in the atmosphere. As such, it is valuable to compare anthropomorphic sources against natural ones to better perceive such estimates.

The meteoroid flux reaching the Earth is of 32.2 metric tons per day when considering that the largest object statistically expected to enter the atmosphere every day is 50 centimeters across [20]. Taking into account a sidereal year and an aluminum mass fraction of 1.2 % in such bodies [18], the mass of aluminum entering the atmosphere from natural sources is approximately 141.1 metric tons per year. The comparison against anthropomorphic sources can be

consulted in Fig. 2, where an average annual increase of 52 % has been observed for satellite-related aluminum injections, while such figure is more reduced for launch vehicles at 14 %. In 2022, anthropomorphic contributions consisted in an excess ratio of 87 %, meaning that the aluminum mass from injected in the atmosphere through the demise of satellite and launch vehicles is just shy of that from natural sources.

Following the estimation of aluminum injections from LEO at the top of the atmosphere, it is important to understand the chemical mechanisms behind the demise process and resolve its byproducts, which is herewith done for anthropomorphic aluminum sources. To ensure that cases A to D are comparable as the domain grows, the number of oxygen-oxygen (O-O) bonds and aluminum-oxygen (Al-O) bonds is monitored throughout the process. Fig. 3 presents the bond count normalized by the total number of atoms as a function of wall time, showing very similar reaction rates as the molecular oxygen interacts with the aluminum structure.

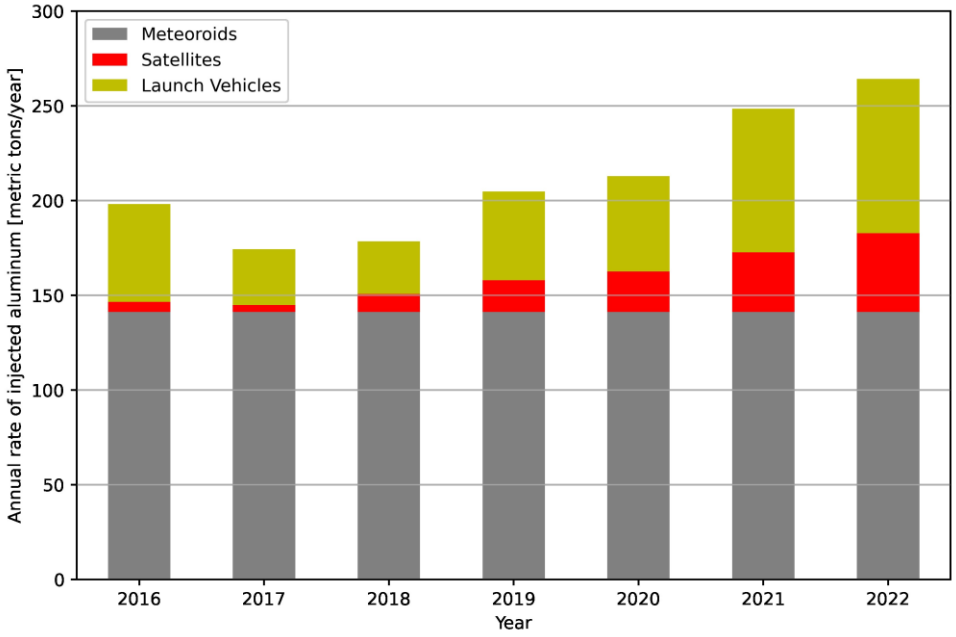


Fig. 2. Annual mass rate of aluminum from LEO reentries: natural and anthropomorphic sources

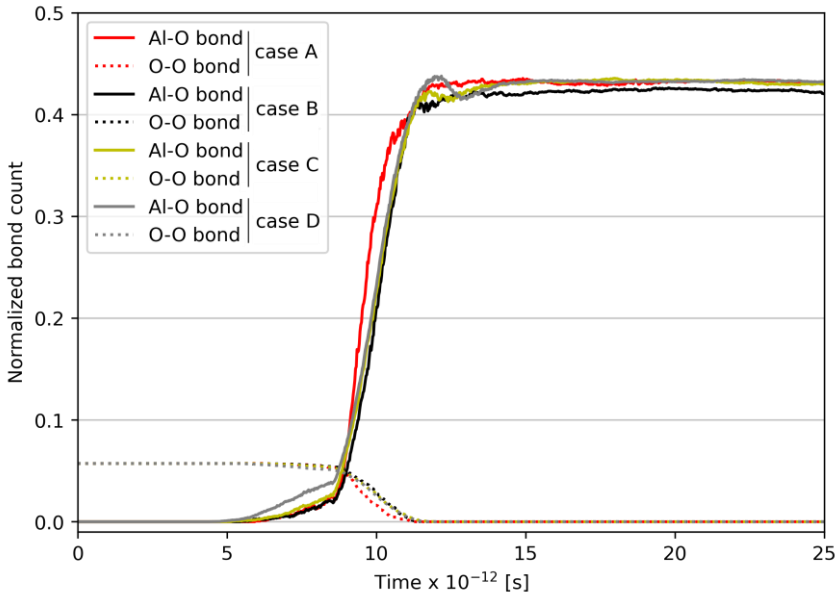


Fig. 3. Time history for the O-O bond breakage and Al-O bond formation

Resorting to the particle position at the last time step of the simulation – also depicted in Fig. 1(iii) – clusters are formed and the aerodynamic diameter computed according to its atomic composition for cases A through D. The histograms are built with bins of $2.5 \times 10^{-10}$ m for both Al and AlO clusters and depict a discrete distribution. Then, the log-normal distribution defined in Equation 2 is fitted to each histogram, as showcased in Fig. 4 for case D. The PDF is presented in Fig. 5 for all cases and the fitted parameters are summarized in Table 3. The expected value for the aerodynamic diameter increases approximately 5.8 % from cases A to D, ranging from 10.6 to $11.2 \times 10^{-10}$ m.

Table 3. Parameters of the log-normal distribution of $X$, and of $d_a$. All values are multiplied by $10^{-10}$ [m].

| Case | $\sigma_X$ | $\mu_X$ | $E(d_a)$ | $M(d_a)$ | $SD(d_a)$ |
|---|---|---|---|---|---|
| A | 0.5046 | 2.235 | 10.617 | 7.247 | 5.717 |
| B | 0.4067 | 2.308 | 10.921 | 8.522 | 4.631 |
| C | 0.4689 | 2.287 | 10.987 | 7.901 | 5.448 |
| D | 0.4945 | 2.296 | 11.230 | 7.781 | 5.911 |

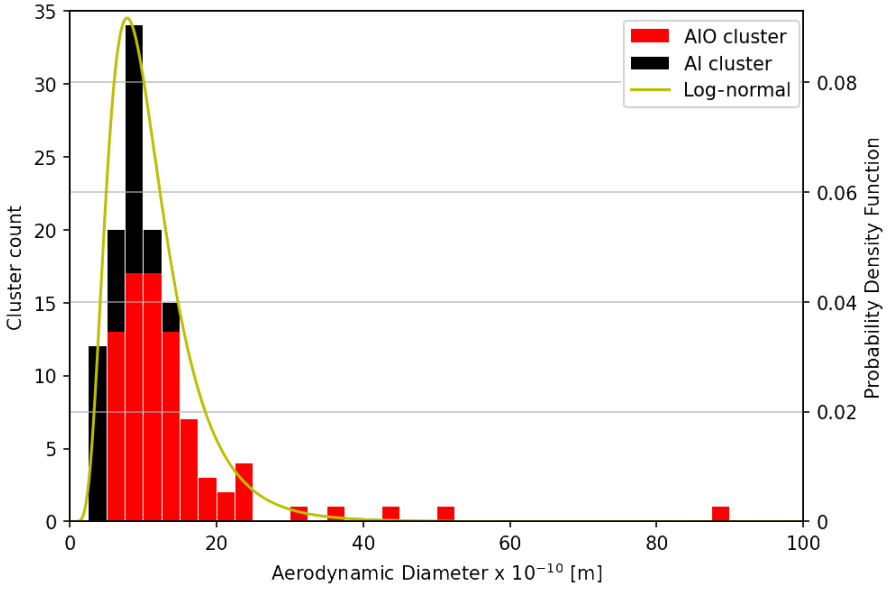

Fig. 4. Discrete count of the aerodynamic diameter for case D with log-normal fitting

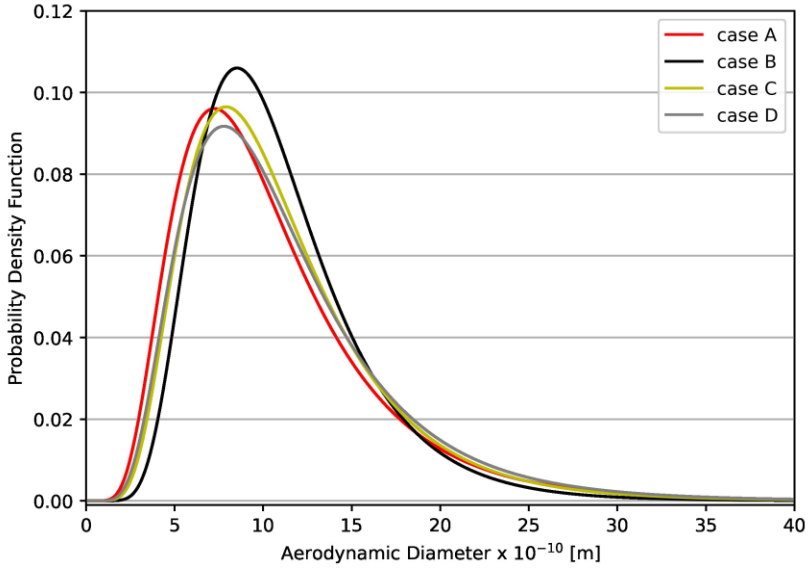

Fig. 5. Log-normal PDF for cases A through D

## 4. DISCUSSION

Firstly, it is important to mention that interpreting the results presented is solely applicable to anthropomorphic objects as they reenter from LEO, while meteoroids enter the atmosphere at much higher speed from unbounded orbits.

The pressing reality showcased in Fig. 2 highlights that the mass rate of aluminum injected at the top of the atmosphere from objects of anthropomorphic origin has almost entirely matched the contribution from natural sources, reaching an excess ratio of 87 %. Such means that the overall yearly mass rate of injected aluminum has practically doubled when compared with that before the *space age*. Despite the largest fraction of anthropomorphic objects being associated with launch vehicles with an annual increase on the aluminum mass rate of 14 %, the contribution of satellite-related debris has increased at a much higher rate of 52 %. Resorting to reentry rate forecasts [4], the contribution from launch vehicles and satellites may respectively reach 500 and 910 metric tons per year, reaching an overall excess ratio 1000 % when compared with natural sources.

As the aforementioned mass of aluminum reenters the atmosphere, byproducts are generated upon a high-temperature oxygen-deficient oxidation reaction. MD simulations take place at very reduced length scales, with a scaling factor to the benchmarking case of $10^{24}$. As such, the results herewith presented aim at showing the scalability of MD simulations in inferring the expected size and settling time of reentry byproducts, which is achieved by increasing the total number of atoms from case A to D in one order of magnitude.

Fig. 3 shows that the reaction rate is kept constant as the domain size grows proportionally in all coordinate directions. The particles bonded into clusters – showcased in Fig. 1(iii) – are categorized and fitted to a log-normal distribution. Note that there is a large portion of aluminum that does not get fully oxidized during the reentry event due to its oxygen deficiency, which can be observed as an outlier in Fig. 4. The large $90 \times 10^{-10}$ m bin presents a large cluster that is mostly made out of aluminum – however, as some oxygen atoms oxidize the surface, it is formally considered an AlO cluster. As such, the aforementioned outlier is not taken into account for the log-normal fitting.

Lastly, Table 3 and Fig. 5 present the results of the scaling methodology. Considering that the expected value increased from 10.6 to $11.2 \times 10^{-10}$ m for a one order of magnitude domain size growth, and assuming either a simple or compound increase rate of 5.8 % per decade, it can be inferred that the expected full-scale aerodynamic diameter figures within the nanoparticle regime with settling time ranging from 25 to 50 years until the upper ozone layer at 40 km of altitude [21]. Aluminum oxides are thought to interact with stratospheric ozone and act as a depletor. Furthermore, the behavior of aluminum and aluminum oxide nanoparticles is not fully understood as to radiative forcing, making its Global Warming Potential an unknown.

It is worth emphasizing that the aforementioned mean values solely communicate the most expected settling time for the clusters described by the log-normal PDF. As such, it allows for a crude approximation of the delay between the mesospheric reentry event and reaching the top of the stratosphere. Nonetheless, the ablation process generates a multitude of clusters: larger ones will sink faster in the atmosphere while smaller nanoparticles may endure for longer or be transported and condensate into larger clusters.

## 5. REMARKS

This study presents developments in the first atomic-scale MD simulation methodology studying the aluminum oxidation process upon mesospheric reentry from LEO, resorting to an empirically-generated interatomic potential between oxygen and aluminum. Large-scale supercomputer runs were carried out to resolve the byproducts of anthropomorphic objects demise and the size of clusters generated. Results show that byproducts arrange into clusters of aluminum oxide and aluminum as the reaction takes place in an oxygen-deficient environment. As such, a large aluminum cluster makes it through the ablation process, while smaller aluminum oxide clusters are created after the impingement of oxygen into the original aluminum structure.

As the total mass of re-entering objects from LEO surpassed 309 metric tons in 2022, the mass of anthropogenically-generated aluminum injected in the atmosphere last year has almost entirely matched the contribution from natural sources such as meteoroids. The results presented show an increase of 5.8 % per decade in the expected value of the characteristic length, showing the scalability of MD simulations, and suggesting that aluminum oxides resulting from

space debris demise in the mesosphere grow into clusters of nanoparticles. These may take an average period of 25 to 50 years decaying in the atmosphere until reaching the upper ozone layer where they can potentially act as an ozone depletor. Nonetheless, smaller nanoparticles – which are generated more frequently – may endure for longer in the atmosphere or be transported and grow into larger clusters.

Future endeavors in this methodology include scaling up the MD simulation domain to the limit of large-scale supercomputing resources so as to more accurately infer the growth rate per decade and define the full-scale expected aerodynamic diameter and settling time.

## ACKNOWLEDGMENTS

This research is funded through the Future Investigators in NASA Earth and Space Science and Technology (FINNEST) fellowship, NASA grant #80NSSC22K1867. The support from Fulbright Portugal through a Fulbright Grant for Graduate Studies – Ph.D. is also acknowledged.

## REFERENCES

[1] P. D. Anz-Meador, J. N. Opiela, D. Shoots and J. C. Liou, "History of On-Orbit Satellite Fragmentations", NASA-TM-2018-220037, 2018.

[2] D. Kessler and B. Cour-Palais, "Collision Frequency of Artificial Satellites: The Creation of a Debris Belt", *Journal of Geophysical Research: Space Physics,* vol. 83, no. A6, pp. 2637-2646, 1978.

[3] ESA Space Debris Office, "ESA's Annual Space Environment Report", GEN-DB-LOG-00288-OPS-SD, 2023.

[4] L. Organski, B. Barber, S. Barkfelt and M. Hobbs, "Environmental Impacts of Satellites from Launch to Deorbit and the Green New Deal for the Space Enterprise", in *AGU Fall Meeting*, 2020.

[5] T. Lips et al., "Assessment of the ATV-1 Re-entry observation campaign for future re-entry missions", in *4th IAASS Conference*, Huntsville, 2010.

[6] S. Bekki et al., "Environmental impacts of atmospheric emissions from spacecraft re-entry demise - Project ATmospheric Impact of SPAcecraft Demise (ATISPADE)", in *ESA Clean Space Industrial Days*, 2021.

[7] S. Bianchi et al., "Atmospheric Re-Entry Assessment (ARA)", in *ESA Clean Space Industrial Days*, 2021.

[8] J. P. Ferreira, Z. Huang, K. Nomura and J. Wang, "Impacts of Satellite Reentry on Atmospheric Composition in the Era of Mega-Constellations: Molecular Dynamics Simulations", in *AGU Fall Meeting 2022*, Chicago, 2022.

[9] J. P. Ferreira, Z. Huang, K. Nomura and J. Wang, "Quantifying Spacecraft Demise Byproducts in the Era of Mega-Constellations", in *73rd International Astronautical Congress*, Paris, 2022.

[10] A. van Duin, "ReaxFF: A Reactive Force Field for Hydrocarbons", *Journal of Physical Chemistry A,* vol. 105, no. 41, pp. 9396-9409, 2001.

[11] S. Hong and A. van Duin, "Molecular dynamics simulations of the oxidation of aluminum nanoparticles using the ReaxFF reactive force field", *The Journal of Physical Chemistry C,* vol. 119, no. 31, pp. 17876-17886, 2015.

[12] K. Nomura, R. Kalia, A. Nakano, P. Rajak and P. Vashishta, "RXMD: A scalable reactive molecular dynamics simulator for optimized time-to-solution", *SoftwareX,* vol. 11, 2020.

[13] D. Thomas and A. Charvet, "An Introduction to Aerosols", in *Aerosol Filtration*, Elsevier, 2017, pp. 1-30.

[14] National Oceanic and Atmospheric Administration, "U. S. Standard Atmosphere", Washington D.C., 1976.

[15] M. Knudsen and S. Weber, "Luftwiderstand gegen die langsame Bewegung kleiner Kugeln", *Annalen der Physik,* vol. 341, no. 15, pp. 981-994, 1911.

[16] A. Stukowski, "Visualization and analysis of atomistic simulation data with OVITO – the Open Visualization Tool", *Modelling and Simulation in Material Sciences and Engineering,* vol. 18, p. 015012, 2010.

[17] J. Wertz, D. Everett and J. Puschell, *Space Mission Engineering: The New SMAD*, Microcosm Press, 2011.

[18] L. Schulz and K. H. Glassmeier, "On the anthropogenic and natural injection of matter into Earth's atmosphere", *Advances in Space Research,* vol. 67, no. 3, pp. 1002-1025, 2021.

[19] L. Anselmo and C. Pardini, "Computational methods for reentry trajectories and risk assessment", *Advances in Space Research,* vol. 35, no. 7, pp. 1343-1352, 2005.

[20] G. Drolshagen et al., "Mass Sccumulation of Earth from Interplanetary Dust, Meteoroids, Asteroids and Comets", *Planetary and Space Science,* vol. 143, pp. 21-27, 2017.

[21] W. J. Randel et al., "Trends in the vertical distribution of ozone", *Science,* vol. 285, no. 5434, pp. 1689-1692, 1999.